Quantum chemical investigations on the superhalogen properties of $Pt(CN)_n$ complexes ($n = 1$–6) and their ability to form new supersalts and superacids: A DFT study

Tabish Rasheed[1], Shamoon Siddiqui[2], Ankit Kargeti[1], Ravikant Shrivastav[1], Dharmesh Shukla[3], Vijay Singh[4], and Anoop Pandey[5]

[1]BML Munjal University
[2]Najran University
[3]GLA University
[4]The University of Dodoma
[5]KS Saket Post Graduate College

April 28, 2020

Abstract

Unique superhalogen properties of $Pt(CN)_n$ complexes ($n = 1$–6) containing cyanide (CN) pseudohalogen moieties bound with platinum (Pt) atom have been investigated under the quantum chemical formalism. The study involves theoretical calculations for both neutral and anionic forms of $Pt(CN)_n$ using density functional theory (DFT) with the hybrid functional B3LYP. In order to improve the accuracy of calculations, 6–311+G(d) basis set was implemented for CN moieties, whereas, SDD basis set supplemented with Stuttgart/Dresden relativistic effective core potential was used for Pt atom. HOMO–LUMO energy band gaps, vibrational frequencies and dissociation energies of $Pt(CN)_n$ complexes have been calculated to investigate their relative stability as well as reactivity. Additionally, superhalogen properties and salt forming capability of $Pt(CN)_n$ complexes have also been analyzed. Focus of analysis is on the delocalization of charges over attached CN ligands in successive members of the $Pt(CN)_n$ species. Reliable low–cost investigations on superacidity properties of associated protonated species have also been carried out keeping their industrial applications in mind.

1. Introduction

In recent times, the scientific community has shown an increased interest in non–halogen electronegative moieties (NHEMs) due to their diverse applications and novel properties. NHEMs act as oxidizing agents in chemical reactions [1–3], play an active role in the formation of novel salts and other compounds [4,5], and are also expected to be useful in future designing of efficient energy storage devices [6]. The general structure of these moieties is $_N$, where, N represents the coordination number satisfying the relation $N \times v_n = v_m + 1$; v_n is normal valence of the ligand atom and v_m is maximal valence of the central atom . Electron affinity (EA) of such chemical species was predicted by Gutsev and Boldyrev [7] to be even higher than the highest atomic EA [5] corresponding to chlorine (3.617 ± 0.003 eV). Due to their ability to display halogen like behavior, they were aptly termed as *superhalogens* . These *superhalogens*usually consist of a central atom , which is a metal corresponding to s or d block elements of the periodic table. The s block elements are capable of binding with a limited number of electronegative atoms due to their fixed valency. However, transition metal atoms having variable oxidation states due to the presence of d orbital, are able to combine with relatively larger number of electronegative species. Workers [5–13] have thoroughly investigated such type of *superhalogens* containing transition metal atoms as the central atom . In such compounds, the transition metal atom combines with other atoms, usually, halogens leading to the

1

formation of strongly bound electronegative species. Current research efforts are directed towards finding novel structural configurations involving alternate atomic combinations, which also satisfy the *superhalogen* criteria [7].

Pseudohalogens are polyatomic molecules that have the capability to form stable negative ions [14,15], just like the halogens. Due to their electronegative nature, these species can acquire an extra electron leading to the formation of negatively charged ions. Hence, these compounds display chemical behavior similar to that of halogens [14,15]. They are constituted of two or more atoms whose bonding remains unchanged during a chemical reaction. The concept of pseudohalogens was introduced in 1925 by Birckenbach [14], who predicted that they have halogen like characteristics and satisfy certain conditions [16,17]. The criteria for a polyatomic molecule to be classified as a pseudohalogen is that, it should be a strongly bound monovalent chemical group, must have the ability to form singly charged anion, and also must be able to combine with hydrogen nucleus to form pseudohalogen–hydrogen acid [16,17]. Workers [18] have particularly concentrated their efforts towards the study of pseudohalogen species such as CN, SCN, OCN, etc. whose anions are more stable as compared to halogens. Superacids corresponding to such chemical groups are combinations of pseudohalogen anions and the hydrogen nucleus [19]. Acidity of superacids was described by Gillespie [20] to be greater than that of 100% sulfuric acid and the Hammett acidity function (H_0) to be lower than –12 [20,21]. Sulfuric acid is considered to be the standard while designating compounds as superacids [22,23]. A technically more accurate description for the strength of superacid is described in terms of Gibbs' free energy change for deprotonation [24,25] which should be lower as compared to that of pure sulfuric acid (302.2 kcal/mol) [26]. As a general measure, compounds having Gibbs' free energy change for deprotonation values lesser than 300 kcal/mol are termed as superacids [27–29]. Olah et al. [30] were the first scientists to report synthesis of a superacid ($FSO_3H \cdot SbF_5$) known as "magic acid". It was composed of a mixture of antimony pentafluoride (SbF_5) and fluorosulfuric acid (HSO_3F) in the molar ratio of 1:1. It has the ability to interact with even hydrocarbons and satisfies the criteria of superacids. Currently, fluoroantimonic acid ($HSbF_6$) is considered to be the strongest superacid [25,26]. Researchers [26,31–38] are actively engaged in the exploration of new superacids which can react even with very weak bases. Such superacids have application in the catalysis and synthesis of compounds particularly those which are useful in medical science [29,39–41]. Research is still ongoing in the search for better superacids. An alternate strategy maybe to use pseudohalogen containing transition metal superhalogens for designing superacids by interacting them with hydrogen nucleus.

The pseudohalogen ligand CN is of particular interest to researchers for use in superhalogens due to their simple structure and ability to combine with various elements. Molecules containing the CN pseudohalogen are found to be having high values of vertical detachment energy (VDE) and hence, have greater probability of displaying superhalogen properties [3]. Samanta et al. [15] have explored the superhalogen properties of $Au(CN)_n$ using theoretical calculations. Smuczyńska et al. [18] have used *ab initio* quantum chemical calculations to predict the properties of $LiX_2{}^-$, $NaX_2{}^-$, $BeX_3{}^-$, $MgX_3{}^-$, $CaX_3{}^-$, $BX_4{}^-$, and $AlX_4{}^-$, where, X represents the CN group. A major benefit of such calculations is their ability to accurately predict superhalogen properties, along with the strength and other traits of corresponding superacid. Experimental laboratory assessment of such superacid is a difficult proposition due to the necessity of heavy–duty apparatus and expertise required in handling them. Computational prediction and analysis of superacid provides important information that maybe useful for chemists involved in chemical synthesis [15]. Previous theoretical investigations [42] have shown that Pt atom can combine with F and Cl to produce superhalogens. Continuing with this line of investigation, the current work aims to study whether the interactions of Pt atom with pseudohalogen CN moieties leads to the formation of superhalogens. It also deals with the in–depth theoretical study of the properties of $Pt(CN)_n$ complexes and their corresponding supersalts and superacids.

2. Computational details

Quantum chemical calculations on $Pt(CN)_n(n = 1–6)$ complexes and their corresponding supersalts and superacids were performed utilizing DFT [43,44] with B3LYP [45,46]. SDD basis set [47,48] supplemented with Stuttgart/Dresden relativistic effective core potential was used for Pt atom, whereas, 6–311+G(d) basis set [49–51] was used for CN moieties. Workers [52,53] have used similar approach to perform geometry

optimizations obtaining better results. All calculations were carried out using the *Gaussian 16W* software package [54] utilizing the linear combination of atomic orbital–molecular orbital (LCAO–MO) technique. In current investigation, all possible minimum energy structures of $Pt(CN)_n$ complexes were modelled. The structures were analyzed by using the GaussView 6 [55] software.

EA values were obtained by calculating the energy difference between optimized structures of neutral and anionic forms of $Pt(CN)_n$ complexes. Highest occupied molecular orbital (HOMO) and lowest unoccupied molecular orbital (LUMO) were visualized by using the GaussView 6 [55] software. The HOMO and LUMO are frontier orbitals which play an important role in determining the chemical reactivity of complexes. Percentage (%) contribution by each element to various orbitals of $Pt(CN)_n$ complexes was determined by using the GaussSum 2.2 [56] program. The program utilizes the output files generated by *Gaussian 16W* software package [54] to determine the elemental percentage (%) contributions in the orbitals. Parameters relevant for probing the properties of supersalts and superacids corresponding to $Pt(CN)_n$ complexes were also calculated by *Gaussian 16W* software package [54] as discussed in following section.

3. Result and discussion

In the present investigation, all probable structures of $Pt(CN)_n$ complexes ($n = 1$–6) were modelled using the GaussView 6 software [55]. The cyanide (CN) moiety is an ambient ligand which interacts with Pt atom through two well–known mechanisms. One of them is through the formation of platinum cyanide complex, in which, C atom of CN moiety bonds with Pt producing Pt–C[?]N. The other one is through creation of platinum iso–cyanide cluster, where, N atom of CN moiety is directly bonded with Pt atom forming Pt–N[?]C. Optimization studies on these isomers indicate that platinum cyanide (PtCN) has lower energy as compared to platinum iso–cyanide complex (PtNC). Hence, the present investigation is primarily focussed towards the study of molecular species containing cyanide (CN) pseudohalogen ligand. The initial geometrical structures of $Pt(CN)_n$ neutral complexes ($n = 1$–6) containing these cyanide (CN) pseudohalogen ligands were optimized using the *Gaussian 16W* software [54]. The final optimized structures of $Pt(CN)_n$ neutral complexes ($n= 1$–6) are shown in Figure 1. It was observed that these complexes have structures similar to those of PtF_n and $PtCl_n$ ($n = 1$–6) complexes [42]. Figure 2 displays optimized geometries of their corresponding anionic complexes along with the bond lengths. On comparing Figures 1 and 2, it was observed that the anionic forms of $Pt(CN)_n$ complexes have geometries similar to neutral complexes with some variations in bond angles and bond lengths. In these complexes, electron configuration of Pt, i.e., [Xe] $4f^{14}5d^9\ 6s^1$ provides a normal valence of 1 which can exceed upto 4 as observed in platinum dioxide (PtO_2) also known as Adams' catalyst [57]. A compound of Pt in higher oxidation state of 6 (PtF_6) has also been chemically synthesized [58], however, it is unstable. In view of these facts, present investigation also aims at exploring the stability of higher order $Pt(CN)_n$ complexes (4 [?]n [?] 6) in addition to the lower order complexes ($n< 4$). In the case of $Pt(CN)_6$, optimization study in the singlet state reveals that after energy minimization, the geometry defaults to a structure similar to $n = 4$ type of $Pt(CN)_n$ complex and NC=CN fragment as provided in the Supporting information sheet (Figure 1S). The complex was then re–optimized in the triplet state providing a stable minimum energy structure. The final obtained geometry of $Pt(CN)_6$ after optimization in triplet state has been included in this work.

It may be observed from Figure 1 that the length of C–N bonds in $Pt(CN)_n$ complexes generally lies in the range 1.16 – 1.18 A. These values are in agreement with the calculated value of C–N bond length in free CN moiety. Hence, it may be inferred that the structure of CN moiety is unaffected when it binds with Pt atom. Pt has oxidation state +1 in Pt(CN) forming a closed shell without any ability to acquire further charge. In the case of $Pt(CN)_2$ complex, a bent structure was found to represent the global minimum on potential energy surface (PES). Optimization of $Pt(CN)_3$ and $Pt(CN)_3-$ complexes provide structures which are approximately in the shape of letter T. In $Pt(CN)_3$ complex, length of Pt–C bonds, which are part of the horizontal arms of the T–shaped structure were equal to 1.98 A. The enclosed C–Pt–C bond angle in this arm was 158.6o. However, length of Pt–C bond in vertical arm of T–shaped structure was 1.87 A. It implies that the bonding between Pt and C is stronger in vertical arm as compared to the horizontal side–arms. Similar observations have been made by Samanta et al. [15] while studying $Au(CN)_n$ complexes. In the case

3

of anionic structure of $Pt(CN)_3$-, length of Pt–C bonds in the horizontal arms of T–shaped structure were 2.01 A, whereas, C–Pt–C bond angle was found to be 172.8deg (Figure 2). These differences in structural parameters of $Pt(CN)_3$ and $Pt(CN)_3$- complexes may be explained by the fact that, in anionic form, the extra electron is delocalized over the entire complex. The $Pt(CN)_4$ complex (Figure 1) exhibits a distorted square geometry in which the C–N bonds are inclined at certain angles with respect to each other. In this structure, one pair of C–N bonds have lengths of 2.01 A and the enclosing C–Pt–C angle has a value of 172.1deg. The other pair of C–N bonds have lengths of 1.92 A with an associated C–Pt–C angle of 95.6deg. Similarly, $Pt(CN)_5$ complex also doesn't have symmetry and it consists of four CN moieties lying in a horizontal plane, whereas, the fifth CN moiety is attached vertically to this plane. In this complex, bond lengths of Pt–C bonds lying in the horizontal plane varies in the range 2.01–2.04 A, whereas, Pt–C bond in vertical plane has length of 1.92 A. In the case of $Pt(CN)_6$, inner d subshell combines with the valence s and p subshells, which, plays an important role in defining the final structure of complex. These hybridized orbitals of Pt have the ability to display an oxidation state of +6 leading to the formation of $Pt(CN)_6$ complex.

Relative stabilities of $Pt(CN)_n$ complexes can be determined by calculating their dissociation energies for fragmentation into $Pt(CN)_{n-1}$ + CN, and $Pt(CN)_{n-2}$ + $(CN)_2$, which are termed as CN and $(CN)_2$ decay channels respectively. Dissociation energies for neutral and anionic complexes are denoted by the terms ΔE_n and ΔE_n^{-} respectively. Table 1 presents the values of ΔE_n and ΔE_n^{-} calculated by utilizing the following expressions:

$\Delta E_n = -\{E[Pt(CN)_n] - E[Pt(CN)_{n-m}] - E[(CN)_m]\}$, $m = 1,2$ (1)

$\Delta E_n^{-} = -\{E[Pt(CN)_n^{-}] - E[Pt(CN)_{n-m}^{-}] - E[(CN)_m]\}$, $m = 1,2$ (2)

Analysis of Table 1 indicates that neutral and anionic $Pt(CN)_n$ complexes are in general stable towards dissociation in CN pathway. ΔE_n values (CN channel) exhibit a general trend of successive decrease for neutral complexes with increasing values of n, except for the case of $n = 4$. Relative stability of these complexes has also been studied by using the *principle of maximum hardness* [59]. According to this principle, absolute hardness (η) is defined by the expression [42]

$\eta = (\epsilon_{LUMO} - \epsilon_{HOMO})/2$. (3)

In above equation, η represents a measure for determining stability of chemical complexes. The complex having the highest value of η is expected to be most stable. ϵ_{HOMO} and ϵ_{LUMO} represent the energies of highest occupied molecular orbital (HOMO) and lowest unoccupied molecular orbital (LUMO) respectively. Using Figure 3 the variation of η with respect to n can be ascertained for neutral $Pt(CN)_n$ complexes. Analyzing the figure, it may be observed that, $Pt(CN)_6$ complex is most stable as per the *principle of maximum hardness* [59]. The HOMO and LUMO plots of $Pt(CN)_6$ complex are shown in Figure 4. The GaussSum 2.2 [56] program has been used to determine the percentage (%) contribution of Pt, C and N atoms towards the LUMO and HOMO of the complexes. The calculated % atomic contribution values for the different complexes are shown in Table 2. The corresponding partial density of states spectra (PDOS) of $Pt(CN)_n$ neutral complexes ($n = 1$–6) denoting the % contribution of different atoms in the molecular orbitals are depicted in Figures 2S(A) – (F) of Supporting information sheet.

Electron affinity (EA) of a compound represents its capability to accept an electron leading to the formation of an anion. In the current investigation, variation of EA values of $Pt(CN)_n$ complexes versus the number of CN moieties has been plotted in Figure 5. The CN moieties have high EA, which enables them to withdraw electrons from Pt in the $Pt(CN)_n$ complexes, providing it with a positive charge. Hence, $Pt(CN)_n$ complexes (n [?] 2) show EA values greater than EA value of chlorine (Figure 5). It may also be observed from Figure 5 that, EA values of $Pt(CN)_n$ complexes with n [?] 5, are higher than even twice the EA value of Cl atom. This observation allows the authors to safely assign $Pt(CN)_n$ complexes with n [?] 2 to the category of superhalogens. Their EA values are also found to be comparable with the EA values of PtF_n complexes [42]. The highest EA value of 7.922 eV was obtained for $Pt(CN)_6$. Figure 5 shows an increasing trend of EA values as the number of cyanide moieties increases in $Pt(CN)_n$ complexes, except for the case of $Pt(CN)_4$, where, the EA value shows an abrupt lowering. Deviation in EA value from the general trend in case of

$Pt(CN)_4$ maybe understood from the fact that platinum has general tendency to exist in oxidation states +2 and +4. The oxidation state +3 for Pt is rare and considered to be unstable. In this state platinum compounds have higher capability of accepting an electron due to unstable nature. Hence, $Pt(CN)_3$ displays an EA value higher than the general trend and thus, EA value of $Pt(CN)_4$ in comparison appears to be lowered.

Single halogen atoms can combine to form diatomic molecules such as Cl_2, F_2, etc. Since, superhalogens mimic the chemical behavior of halogens, they must also be able to form dimers. In order to probe this aspect of $Pt(CN)_n$ superhalogens, the authors have considered the test case of $Pt(CN)_4$. Investigation on dimer of $Pt(CN)_4$ superhalogens was conducted by choosing two initial geometries. In the first configuration, both complexes were positioned parallel to each other in such a manner that the Pt atom of one complex was closer to CN moieties of the other complex and vice versa. In the second configuration, planes of both complexes were set perpendicular to each other under the constraint that Pt and CN were adjacent to each other. After geometry optimization, it was observed that the first configuration had higher stability. Optimized geometrical structure of this stable configuration of dimer and corresponding HOMO and LUMO plots are shown in Figures 6 and 7 respectively. Stability of dimer was determined by analyzing normal mode frequencies, binding energies and HOMO–LUMO gaps. Frequencies corresponding to all the normal modes have real values. The binding energy of $[Pt(CN)_4]_2$ is 2.37 eV, which is greater than the binding energy of F_2 molecule (1.21 eV) and also the binding energy of $(PtF_4)_2$ i.e., 1.72 eV [42]. An interesting point to be noted from the HOMO and LUMO orbitals (Figure 7) is that they are distributed over the entire dimer.

In order to understand the nature of supersalts of $Pt(CN)_n$ superhalogen complexes, interaction between K and $Pt(CN)_4$ was studied. An initial geometry consisting of K atom placed above the Pt atom of $Pt(CN)_4$ was provided to *Gaussian 16W* software for optimization. After geometry optimization, K atom was found to be displaced from its original position to a side position (Figure 8). Normal mode analysis predicted that all frequencies were real, so, the supersalt is expected to be stable. Figure 9 displays HOMO and LUMO of the supersalt K– $Pt(CN)_4$. In this figure, it may be observed that both HOMO and LUMO are spread over the entire supersalt complex, except over the K atom. Similar study for the case of KF reveals that HOMO doesn't contribute to K site, however, LUMO contribute to K site.

Superacidity properties of hydrogenated $Pt(CN)_n$ complexes represented as $H–Pt(CN)_n$, have been analyzed for the corresponding energy minimum structures. These optimized structures of $H–Pt(CN)_n$ are displayed in Figure 10. In these hydrogenated $Pt(CN)_n$ complexes, bond length of Pt–CNH bond was found to have increased in comparison with Pt–CN bond. Bond length of H–CN bond in the species $H–Pt(CN)_n$, for $n = 2–6$, lies in the range $0.99 – 1.0$ Å, which is comparable with the bond length of H–CN in free state. These observations lead to the conclusion that HCN moiety weekly interacts with the central Pt atom in $H–Pt(CN)_n$. In the protonated $Pt(CN)_n$ species, bond length of C–N bond is almost equal to the bond length of C–N bond in free cyanide molecule.

An important concept which has been widely accepted as a tool for prediction of relative strength of superacids is gas–phase acidity (GPA). GPA for a superacid can be obtained by calculating the changes in Gibbs' free energies ($[?]G_{depro}$) due to deprotonation chemical reactions and is defined as $1/[?]G_{depro}$. Researchers consider a molecular species to be in the category of superacids, if the $[?]G_{depro}$ value is less than 300 kcal/mol [27–29]. The calculated values of HOMO–LUMO energy band gap ($[?]E_{gap}$) and $[?]G_{depro}$ for $H–Pt(CN)_n$ species are listed in Table 3. $[?]G_{depro}$ has been calculated by utilizing the below mentioned equation:

$$\Delta G_{depro} = \Delta G\,[Pt(CN)_n{}^-] + \Delta G\,[H^+] - \Delta G\,[H–Pt(CN)_n], \quad (4)$$

where, ΔG denotes the change in Gibbs' free energy which includes thermal enthalpy and entropy terms at 298.15 K. The value of $G\,[H^+] = -6.3$ kcal/mol has been taken from literature [27,60]. From Table 3, it may be observed that the values of $[?]G_{depro}$ for $H–Pt(CN)_n$, when $n = 2–6$ are lower as compared to $[?]G_{depro}$ value of H_2SO_4 (302.2 kcal/mol) [26]. It may also be noted that, $[?]G_{depro}$ value of the strongest superacid $HSbF_6$ is 255.5 kcal/mol [27]. The $[?]G_{depro}$ value of $HSbF_6$ is 7.6492 kcal/mol and 4.6611 kcal/mol greater as compared to the corresponding values of $H–Pt(CN)_5$ and $H–Pt(CN)_6$ respectively. Hence, these two

5

superacids viz. $H–Pt(CN)_5$ and $H–Pt(CN)_6$ are predicted to be stronger than the strongest superacid $HSbF_6$. $[?]G_{depro}$ values of $H–Pt(CN)_n$ for $n = 2–6$ are also found to be lower as compared to the corresponding values of H_2SO_4 [26], HNO_3 [26] and HCl [25,61]. Hence, considering these results, it may be proposed that, superhalogen anions $Pt(CN)_n{}^-$ with $n = 2–6$, can be used to develop a new class of superacids. Relative chemical reactivity of molecular species can be predicted through analysis of HOMO–LUMO energy band gap (ΔE_{gap}) values provided in Table 3. It is interesting to note that, ΔE_{gap} values of odd order superacids are greater than previous even order superacids. In Figure 11, the HOMO–LUMO plots for $H–Pt(CN)_5$ are shown. From these plots, it is observed that, HOMO covers almost the entire complex except the HCN portion, however, LUMO is spread over the complete complex. It reinforces the fact that the nature of bonding is electrovalent.

In order to substantiate the current investigation, correlation plot of GPA (calculated as $1/[?]G_{depro}$) of $H–Pt(CN)_n$ species versus vertical detachment energy (VDE) of corresponding $Pt(CN)_n{}^-$ anions has been drawn as shown in Figure 12. VDEs of $Pt(CN)_n{}^-$ anions have been calculated by using the following equation

$$VDE = E[Pt(CN)_n]_{SP} – E[Pt(CN)_n{}^-]_{Opt},$$

where, $E[Pt(CN)_n{}^-]_{Opt}$ represents the total energy of optimized anions and $E[Pt(CN)_n]_{SP}$ denotes the single point energies of neutral compounds whose structural parameters are same as that of corresponding optimized anion geometries [25]. In Figure 12, a linear relationship is found to exist for the best fit line between GPA $(1/[?]G_{depro})$ x 10^{-2} (in eV^{-1}) of $H–Pt(CN)_n$ species and VDE (in eV) of corresponding $Pt(CN)_n$-anions expressed in the form:

GPA $(1/[?]G_{depro})$ x $10^{-2} = 0.39898$ x VDE $+ 5.96849$.

The correlation coefficient $r = 0.9834$ calculated for the linear relationship suggests a strong positive linear relationship as described by Ratner [62].

4. Conclusions

Superhalogen behavior of $Pt(CN)_n$ complexes was studied using DFT(B3LYP) and 6–311+G(d) basis set for CN moieties, along with the SDD basis set supplemented with Stuttgart/Dresden relativistic effective core potential for Pt atom. These complexes exhibit successively increasing EA values for increasing values of n, reaching a peak value of 7.922 eV for $Pt(CN)_6$. The EA of $Pt(CN)_6$ complex is more than double the EA value of chlorine. Superhalogen property of $Pt(CN)_n$ complexes is based on delocalization of charges over attached CN pseudo ligands. The nature of bonding in dimer of $Pt(CN)_4$ was found to be similar to that of halogen dimer. The binding energy of $K–Pt(CN)_4$ is larger than that of KF suggesting that a new class of salt can be synthesized by reacting $Pt(CN)_4$ with K. $H–Pt(CN)_n$ chemical species are expected to behave as a superacids for $n = 2–6$, with $H–Pt(CN)_5$ and $H–Pt(CN)_6$ predicted to be stronger acids as compared to the strongest superacid $HSbF_6$. GPA $(1/[?]G_{depro})$ of $H–Pt(CN)_n$ superacids and VDE of corresponding $Pt(CN)_n$- anions are found to exhibit a linear relationship with correlation coefficient $r = 0.9834$.

Conflict of Interest

The authors declare no conflict of interest.

References

[1] N. Bartlett, G. Lucier, C. Shen, W. J. Casteel Jr., L. Chacon, J. Munzenberg, B. Zemva, *J. Fluor. Chem.* **1995** , *71* , 163–164.

[2] F. Arnold, *Nature* **1980** , *284* , 610–611.

[3] L.–P. Ding, P. Shao, C. Lu, F.–H. Zhang, Y. Liu and Q. Mu, *Inorg. Chem.* **2017** , *56* , 7928–7935.

[4] T. Rasheed, S. A. Siddiqui, N. Bouarissa, *J. Fluor. Chem.* **2013** , *146* , 59–65.

[5] T. Rasheed, S. A. Siddiqui, A. K. Pandey, N. Bouarissa, A. Al–Hajry, *J. Fluor. Chem.* **2017** , *195* , 85–92.

[6] P. Jena, *J. Phys. Chem. Lett.* **2015** , *6* , 1119-1125.

[7] G. L. Gutsev, A. I. Boldyrev, *Chem. Phys.* **1981** , *56* , 277–283.

[8] G. L. Gutsev, B. K. Rao, P. Jena, X. B. Wang, L. S. Wang, *Chem. Phys. Lett.* **1999** , *312* , 598–605.

[9] G. L. Gutsev, S. N. Khanna, B. K. Rao, P. Jena, *Phys. Rev. A* **1999** , *59* , 3681–3684.

[10] M. K. Scheller, R. N. Compton, L. S. Ceederbaum, *Science* **1995** , *270* , 1160–1166.

[11] R. N. Compton, P. W. Reinhardt, *J. Chem. Phys.* **1980** , *72* , 4655–4656.

[12] O. Graudejus, S. H. Elder, G. M. Lucier, C. Shen, N. Bartlett, *Inorg. Chem.* **1999** , *38* , 2503–2509.

[13] G. M. Lucier, C. Shen, S. H. Elder, N. Bartlett, *Inorg. Chem.* **1998** , *37* , 3829–3834.

[14] L. Birckenbach, K. Kellermann, *Ber. Dtsch. Chem. Ges.* **1925** , *58* , 786–794.

[15] D. Samanta, M. M. Wu, P. Jena, *Inorg. Chem.* **2011** , *50* , 8918–8925.

[16] A. M. Golub, H. Köhler, V. V. Stopenko, Chemistry of Pseudohalides; Elsevier: Amsterdam, **1986** .

[17] H. Brand, A. Schulz, A. Villinger, *Z. Anorg. Allg. Chem.* **2007** , *633* , 22–35.

[18] S. Smuczyńska, P. Skurski, *Inorg. Chem.* **2009** , *48* , 10231–10238.

[19] A. K. Srivastava, N. Misra, *Polyhedron* **2015** , *102* , 711-714.

[20] R. J. Gillespie, T. E. Peel, E. A. Robinson, *J. Am. Chem. Soc.* **1971** , *93* , 5083-5087.

[21] R. J. Gillespie, T. E. Peel, *J. Am. Chem. Soc.* **1973** , *95* , 5173-5178.

[22] R. J. Gillespie, T. E. Peel, *Adv. Phys. Org. Chem.* **1971** , *9* , 1–24.

[23] A. A. Viggiano, M. J. Henchman, F. Dale, C. A. Deakyne, J. F. Paulson, *J. Am. Chem. Soc.* **1992** , *114* , 4299–4306.

[24] A. K. Srivastava, A. Kumar, N. Misra, *J. Fluor. Chem.* **2017** , *197* , 59–62.

[25] A. K. Srivastava, A. Kumar, N. Misra, *New J. Chem.* **2017** , *41* , 5445–5449.

[26] I. A. Koppel, P. Burk, I. Koppel, I. Leito, T. Sonoda, M. Mishima, *J. Am. Chem. Soc.* **2000** , *122* , 5114–5124.

[27] M. Czapla, P. Skurski, *Chem. Phys. Lett.* **2015** , *630* , 1-5.

[28] M. Czapla, I. Anusiewicz, P. Skurski, *Chem. Phys.* **2016** , *465-466* , 46-51.

[29] F.–Q. Zhou, W.–H. Xu, J.–F. Li, R.–F. Zhao, B. Yin, *Inorg. Chem.* **2017** , *56* , 11787–11797.

[30] G. A. Olah, R. H. Schlosberg, *J. Am. Chem. Soc.* **1968** , *90* , 2726–2727.

[31] R. J. Gillespie, T. E. Peel, *Adv. Phys. Org. Chem.* **1971** , *9* , 1–24.

[32] A. H. Otto, T. Steiger, S. Schrader, *Chem. Commun.* **1998** , *3* , 391–392.

[33] S. Senger, L. Radom, *J. Phys. Chem. A* **2000** , *104* , 7375–7385.

[34] G. Zhong, B. Chan, L. Radom, *Org. Lett.* **2009** , *11* , 749–751.

7

[35] K. E. Gutowski, D. A. Dixon, *J. Phys. Chem. A* **2006** , *110* , 12044–12054.

[36] J. Axhausen, C. Ritter, K. Lux, A. Kornath, *Z. Anorg. Allg. Chem.* **2013** , *639* , 65–72.

[37] J. Axhausen, K. Lux, A. Kornath, *Angew. Chem. Int. Ed.* **2014** , *53* , 3720–3721.

[38] C. Bour, R. Guillot, V. Gandon, *Chem. Eur. J.* **2015** , *21* , 6066–6069.

[39] H. Pines, The Chemistry of Catalytic Hydrocarbon Conversions; Academic Press: New York, **1981** .

[40] J. Fahy, A. Duflos, J.–P. Ribet, J.–C. Jacquesy, C. Berrier, M.–P. Jouannetaud, F. Zunino, *J. Am. Chem. Soc.* **1997** ,*119* , 8576-8577.

[41] L. J. C. B. Milandou, H. Carreyre, S. Alazet, G. Greco, A. M.–Mingot, C. N. Loumpangou, J.–M. Ouamba, F. Bouazza, T. Billard, S. Thibaudeau, *Angew. Chem. Int. Ed.* **2017** , *56* , 175–178.

[42] S. A. Siddiqui, T. Rasheed, A. K. Pandey, *Comp. Theo. Chem.* **2012** , *979* , 119–127.

[43] P. Hohenberg, W. Kohn, *Phys. Rev.* **1964** ,*136* , B864–B871.

[44] T. Ziegler, *Chem. Rev.* **1991** , *91* , 651–667.

[45] A. D. Becke, *J. Chem. Phys.* **1993** , *98* , 1372–1377.

[46] A. D. Becke, *J. Chem. Phys.* **1993** , *98* , 5648–5652.

[47] P. Schwerdtfeger, M. Dolg, W. H. E. Schwarz, G. A. Bowmaker, P. D. W. Boyd, *J. Chem. Phys.* **1989** , *91* , 1762–1774.

[48] M. Dolg, U. Wedig, H. Stoll, H. Preuss, *J. Chem. Phys.* **1987** , *86* , 866–872.

[49] R. Krishnan, J. S. Binkley, R. Seeger, J. A. Pople, *J. Chem. Phys.* **1980** , *72* , 650–654.

[50] A. D. Mclean, G. S. Chandler, *J. Chem. Phys.* **1980** , *72* , 5639–5648.

[51] L. A. Curtiss, M. P. McGrath, J. P. Blaudeau, N. E. Davis, R. C. Binning Jr., L. Radom, *J. Chem. Phys.* **1995** ,*103* , 6104–6113.

[52] M. Willis, M. Gotz, A. K. Kandalam, G. F. Gantefor, P. Jena,*Angew. Chem. Int. Ed.* **2010** , *49* , 8966–8970.

[53] M. M. Wu, H. P. Wang, Y. J. Ko, Q. A. Wang, Q. A. Sun, B. Kiran, A. K. Kandalam, K. H. Bowen, P. Jena, *Angew. Chem. Int. Ed.* **2011** , *50* , 2568–2572.

[54] Gaussian 16, Revision C.01, M. J. Frisch, G. W. Trucks, H. B. Schlegel, G. E. Scuseria, M. A. Robb, J. R. Cheeseman, G. Scalmani, V. Barone, G. A. Petersson, H. Nakatsuji, X. Li, M. Caricato, A. V. Marenich, J. Bloino, B. G. Janesko, R. Gomperts, B. Mennucci, H. P. Hratchian, J. V. Ortiz, A. F. Izmaylov, J. L. Sonnenberg, D. Williams–Young, F. Ding, F. Lipparini, F. Egidi, J. Goings, B. Peng, A. Petrone, T. Henderson, D. Ranasinghe, V. G. Zakrzewski, J. Gao, N. Rega, G. Zheng, W. Liang, M. Hada, M. Ehara, K. Toyota, R. Fukuda, J. Hasegawa, M. Ishida, T. Nakajima, Y. Honda, O. Kitao, H. Nakai, T. Vreven, K. Throssell, J. A. Montgomery, Jr., J. E. Peralta, F. Ogliaro, M. J. Bearpark, J. J. Heyd, E. N. Brothers, K. N. Kudin, V. N. Staroverov, T. A. Keith, R. Kobayashi, J. Normand, K. Raghavachari, A. P. Rendell, J. C. Burant, S. S. Iyengar, J. Tomasi, M. Cossi, J. M. Millam, M. Klene, C. Adamo, R. Cammi, J. W. Ochterski, R. L. Martin, K. Morokuma, O. Farkas, J. B. Foresman, and D. J. Fox, Gaussian, Inc., Wallingford CT, **2016** .

[55] GaussView, Version 6.1, Roy Dennington, Todd A. Keith, and John M. Millam, Semichem Inc., Shawnee Mission, KS, **2016** .

[56] N. M. O'Boyle, A. L. Tenderholt, K. M. Langner, *J. Comp. Chem.* **2008** , *29* , 839–845.

[57] V. Voorhees, R. Adams, *J. Am. Chem. Soc.* **1922** ,*44* , 1397–1405.

[58] B. Weinstock, H. H. Claassen, J. G. Malm, *J. Am. Chem. Soc.* **1957** , *79* , 5832–5832.

[59] R. G. Pearson, *Acc. Chem. Res.* **1993** , *26* , 250–255.

[60] I. A. Topol, G. J. Tawa, S. K. Burt, A. A. Rashin, *J. Phys. Chem. A* **1997** , *101* , 10075–10081.

[61] J. E. Bartmess, In Negative Ion Energetics Data in NIST Standard reference Database Number 69; W. G. Mallard, P. J. Linstrom, Eds.; National Institute of Standards and Technology, Gaithersburg, MD, **1997** .

[62] B. Ratner, *J. Target. Meas. Anal. Mark.* **2009** ,*17* , 139–142.

Table 1. Dissociation energies (in eV) ΔE_n and ΔE_n^- of various fragments of $Pt(CN)_n$ and $Pt(CN)_n^-$ (n = 1–6) clusters respectively calculated by combination of DFT (B3LYP) method and pseudo basis set.

Neutral cluster	Neutral cluster	Neutral cluster	Anionic cluster	Anionic cluster	Anionic cluster
Species	ΔE_n (eV) [CN dissociation channel]	ΔE_n (eV) [$(CN)_2$ dissociation channel]	Species	ΔE_n^- (eV) [CN dissociation channel]	ΔE_n^- (eV) [$(CN)_2$ dissociation channel]
$Pt(CN)$	0.1717	–	$Pt(CN)^-$	0.2028	–
$Pt(CN)_2$	0.1452	0.0866	$Pt(CN)_2^-$	0.1724	0.1449
$Pt(CN)_3$	0.0818	-0.0033	$Pt(CN)_3^-$	0.1621	0.1043
$Pt(CN)_4$	0.1083	-0.0402	$Pt(CN)_4^-$	0.1000	0.0319
$Pt(CN)_5$	0.0552	-0.0667	$Pt(CN)_5^-$	0.1188	-0.0114
$Pt(CN)_6$	0.0510	-0.1240	$Pt(CN)_6^-$	0.0577	-0.0538

Table 2. Percentage contribution of Pt, C and N in frontier orbitals in neutral forms of $Pt(CN)_n$ (n = 1–6).

Species	Frontier orbitals	Symmetry[a]	% contribution[b,c] Pt	% contribution[b,c] C	% contribution[b,c] N
$Pt(CN)$	LUMO HOMO	$C_{[?]v}$	82(α), 100(β) 30(α), 81(β)	12(α), 0(β) 27(α), 14(β)	7(α), 0(β) 42(α), 5(β)
$Pt(CN)_2$	LUMO HOMO	C_1	43 82	39 12	18 6
$Pt(CN)_3$	LUMO HOMO	C_s	49(α), 29(β) 33(α), 35(β)	27(α), 26(β) 22(α), 21(β)	24(α), 46(β) 45(α), 44(β)
$Pt(CN)_4$	LUMO HOMO	C_1	37 12	33 37	29 51
$Pt(CN)_5$	LUMO HOMO	C_1	44(α), 12(β) 8(α), 4(β)	27(α), 35(β) 42(α), 43(β)	30(α), 53(β) 51(α), 53(β)
$Pt(CN)_6$	LUMO HOMO	C_1	44(α), 10(β) 0(α), 0(β)	54(α), 36(β) 40(α), 43(β)	2(α), 54(β) 60(α), 57(β)

[a] Point groups for higher n (>3) values are taken to be C_1 for structural optimization purpose.

[b] α and β refer to alpha and beta molecular orbitals corresponding to unrestricted calculations. [c]Percentage contributions from Pt, C and N atoms in the frontier orbitals of neutral forms of $Pt(CN)_n$ (n = 1–6) have been rounded.

Table 3. Calculated values of HOMO–LUMO energy band gap (ΔE_{gap}) and free energy change for deprotonation ($[?]G_{depro}$) for H–Pt(CN)$_n$ ($n = 1$–6).

Species	Symmetry	$\Delta E_{\gamma\alpha\pi}$ (ε'')	$[?]G_{depro}$ (kcal/mol)
H–Pt(CN)	$C_{[?]v}$	3.7024	313.4748
H–Pt(CN)$_2$	C_s	2.0065	282.8423
H–Pt(CN)$_3$	C_{2v}	3.6950	271.5955
H–Pt(CN)$_4$	C_1	1.9839	265.4335
H–Pt(CN)$_5$	C_1	3.5478	247.8508
H–Pt(CN)$_6$	C_1	1.0604	250.8389
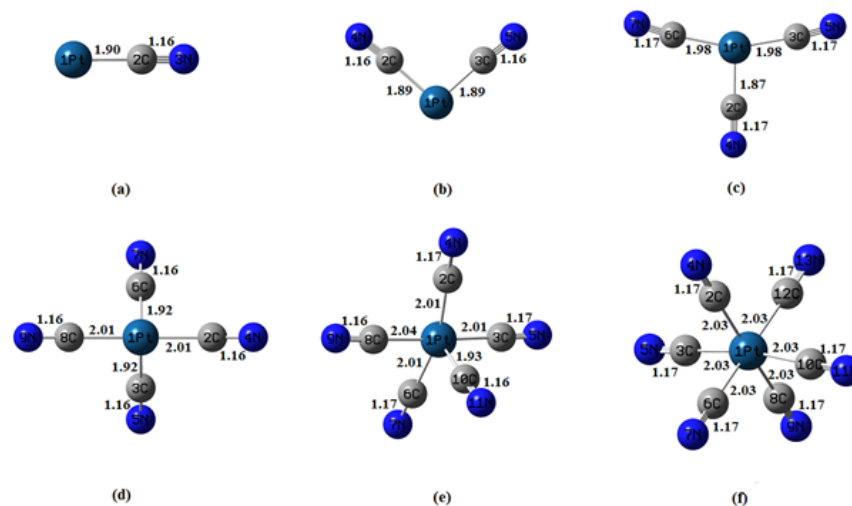
Figure 1. Equilibrium geometries of neutral Pt(CN)$_n$ ($n = 1$–6) complexes showing their bond lengths (in Å).
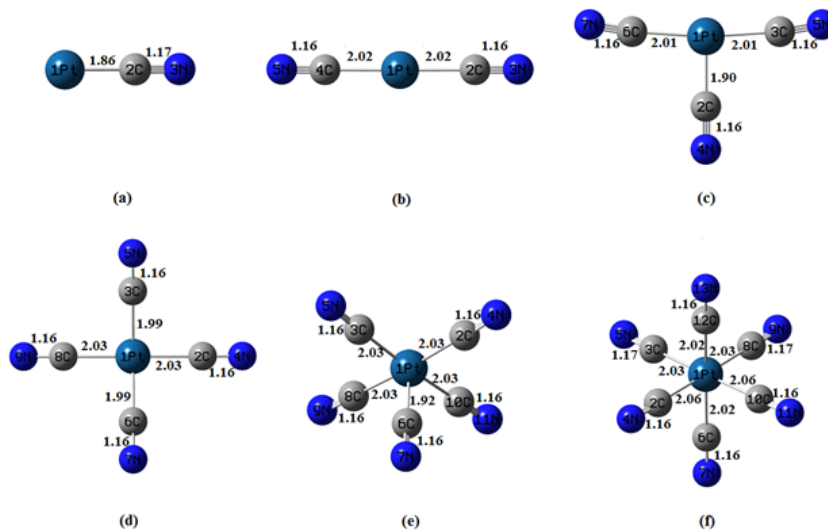
Figure 2. Equilibrium geometries of anionic $Pt(CN)_n$ ($n = 1–6$) complexes showing their bond lengths (in Å).
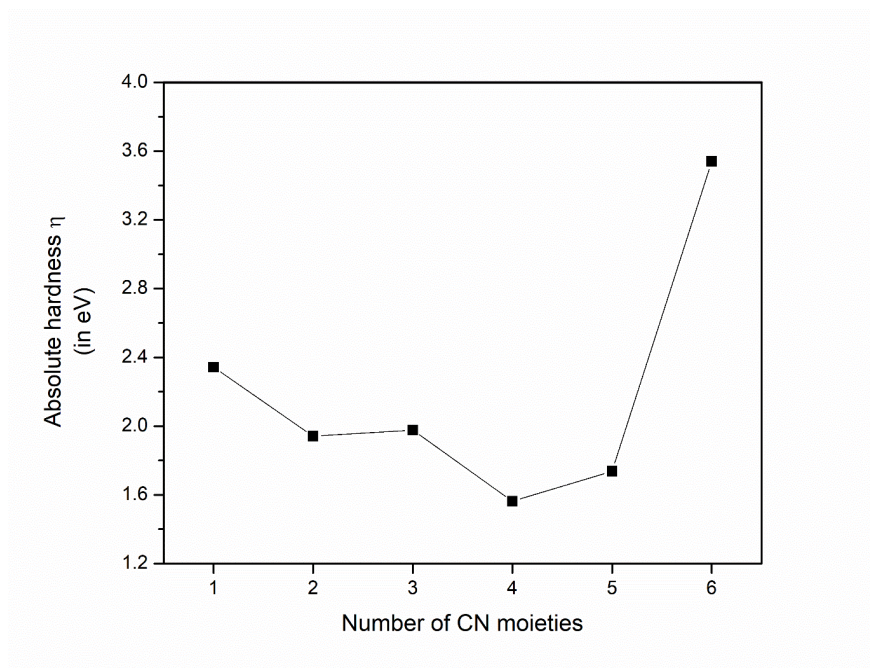
Figure 3. Absolute hardness η of $Pt(CN)_n$ complexes ($n = 1–6$) calculated using DFT (B3LYP) method.

11
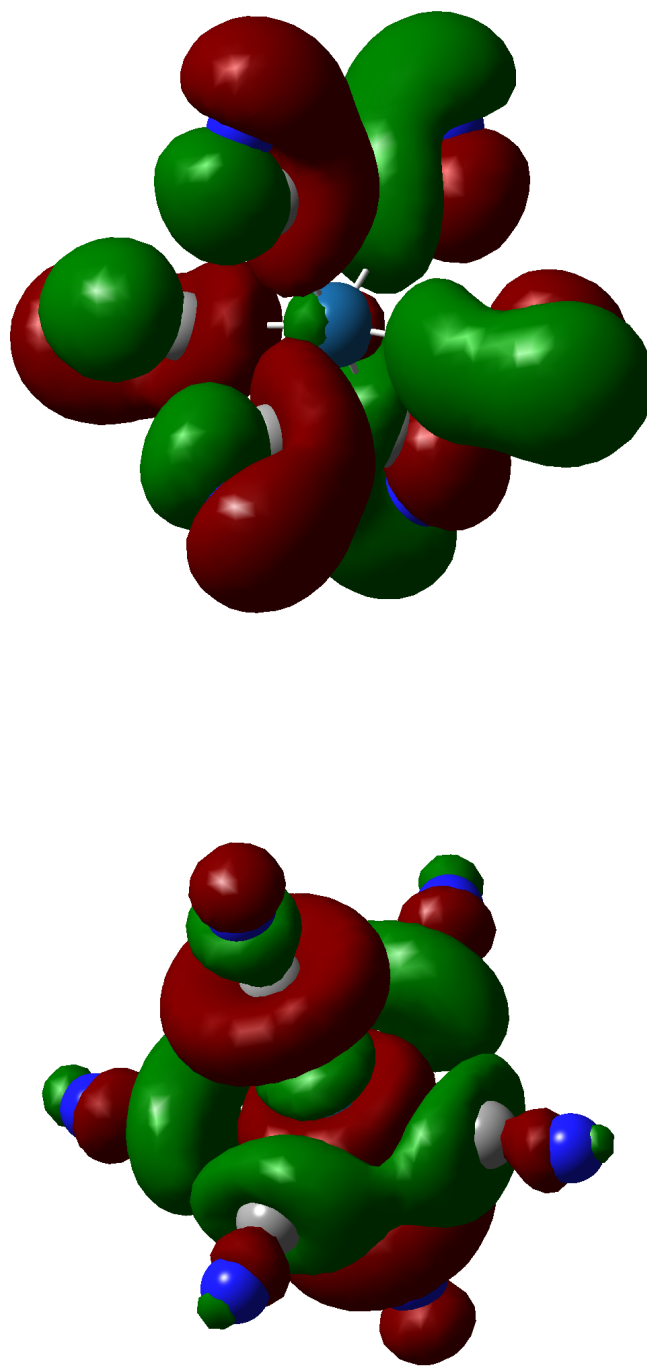
HOMO LUMO

Figure 4. HOMO–LUMO surfaces of $Pt(CN)_6$ superhalogen calculated using DFT (B3LYP) method.
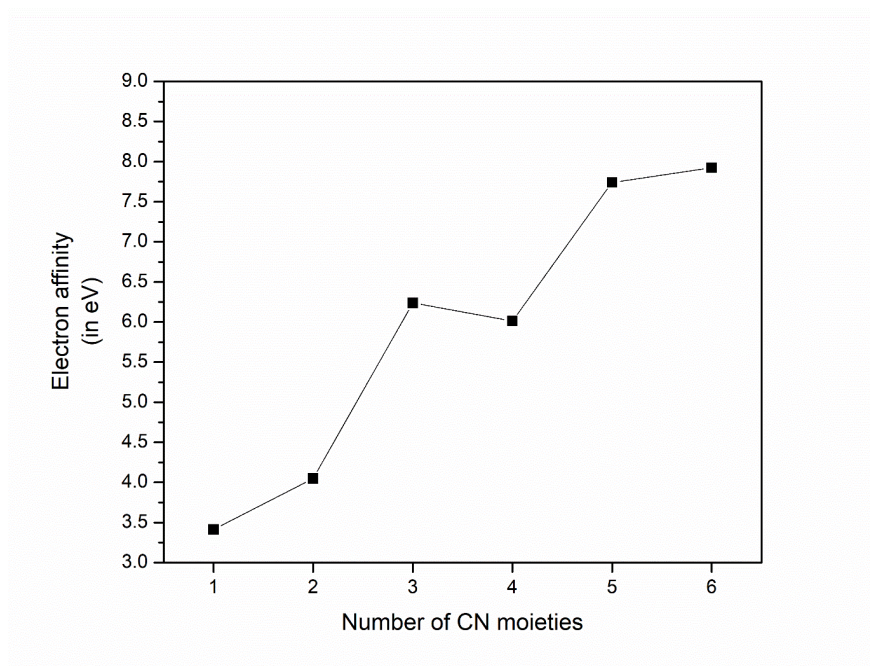
Figure 5. Electron affinity of $Pt(CN)_n$ complexes ($n = 1$–6) as a function of n .
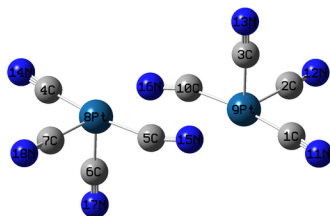
Figure 6. Optimized geometry of dimer formed of two $Pt(CN)_4$ complexes.

13
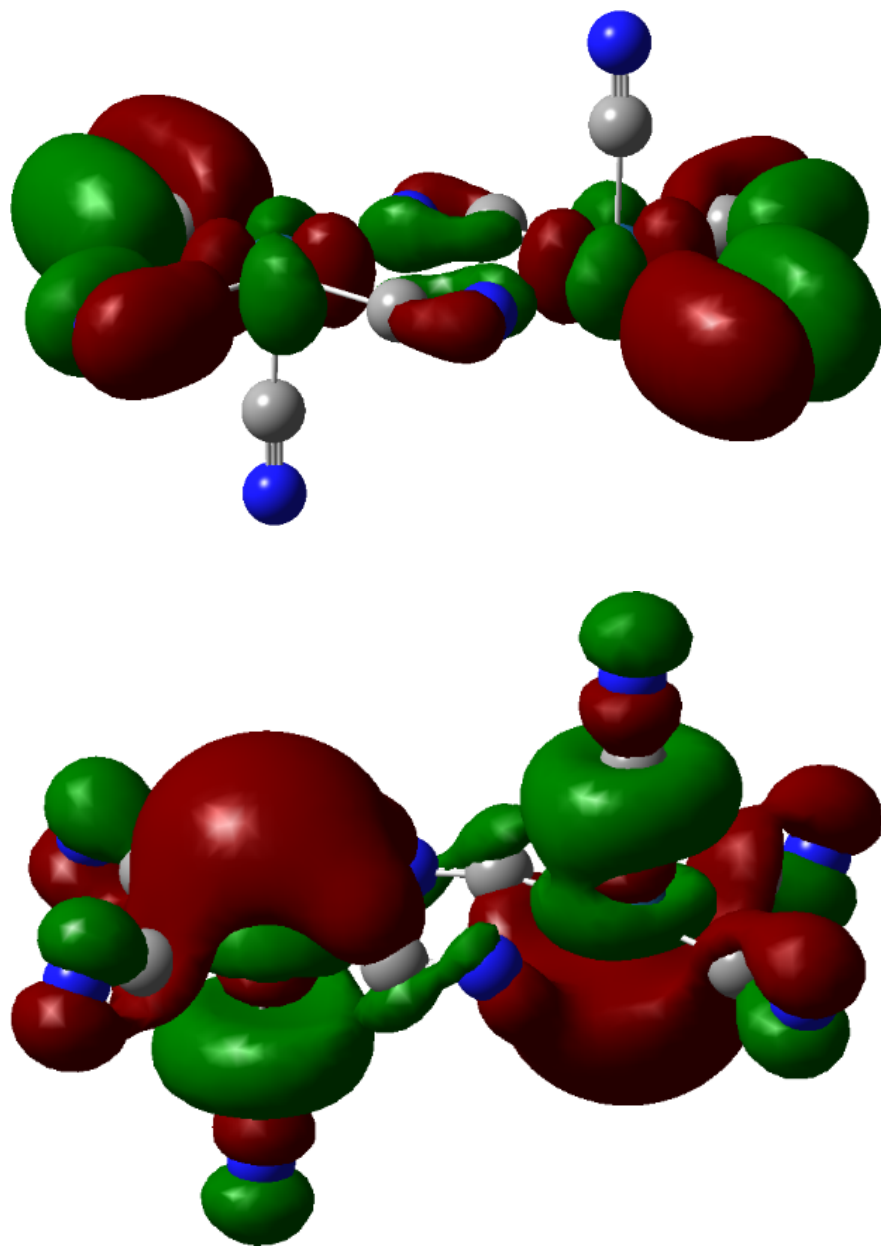
HOMO LUMO

Figure 7. HOMO and LUMO plots of dimer formed of two $Pt(CN)_4$ complexes.
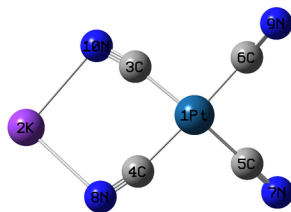
Figure 8. Optimized geometry of supersalt K–Pt(CN)$_4$.
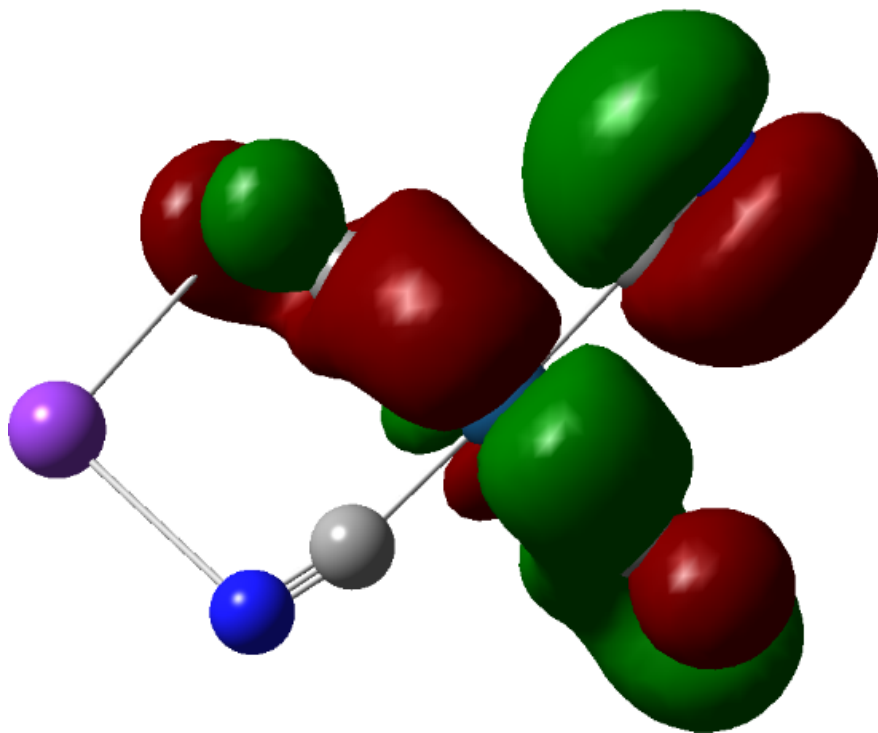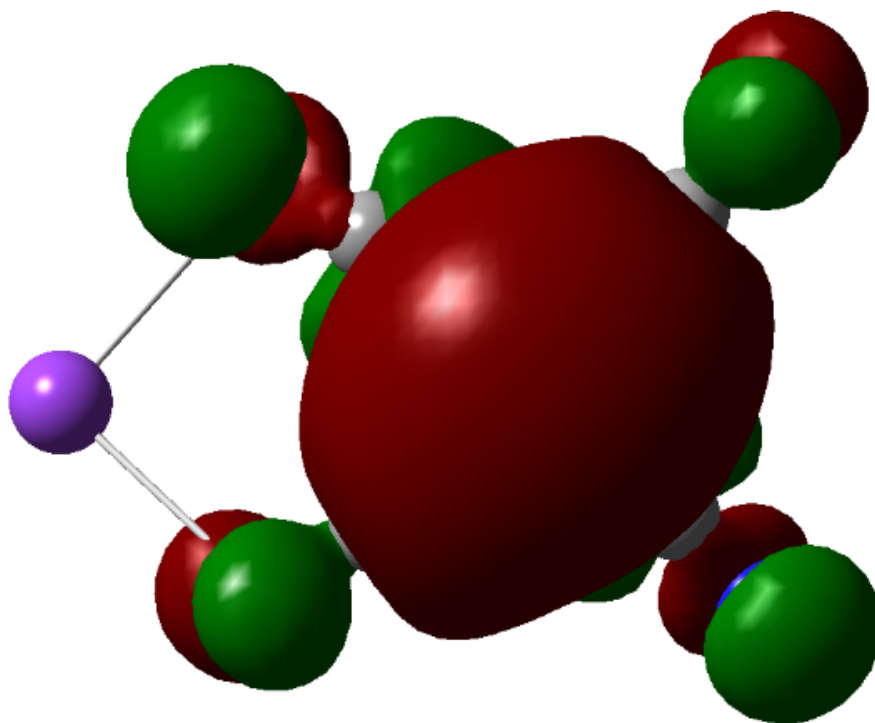
HOMO LUMO

Figure 9. HOMO and LUMO plot of the optimized geometry of supersalt formed due to interaction between K and $Pt(CN)_4$.
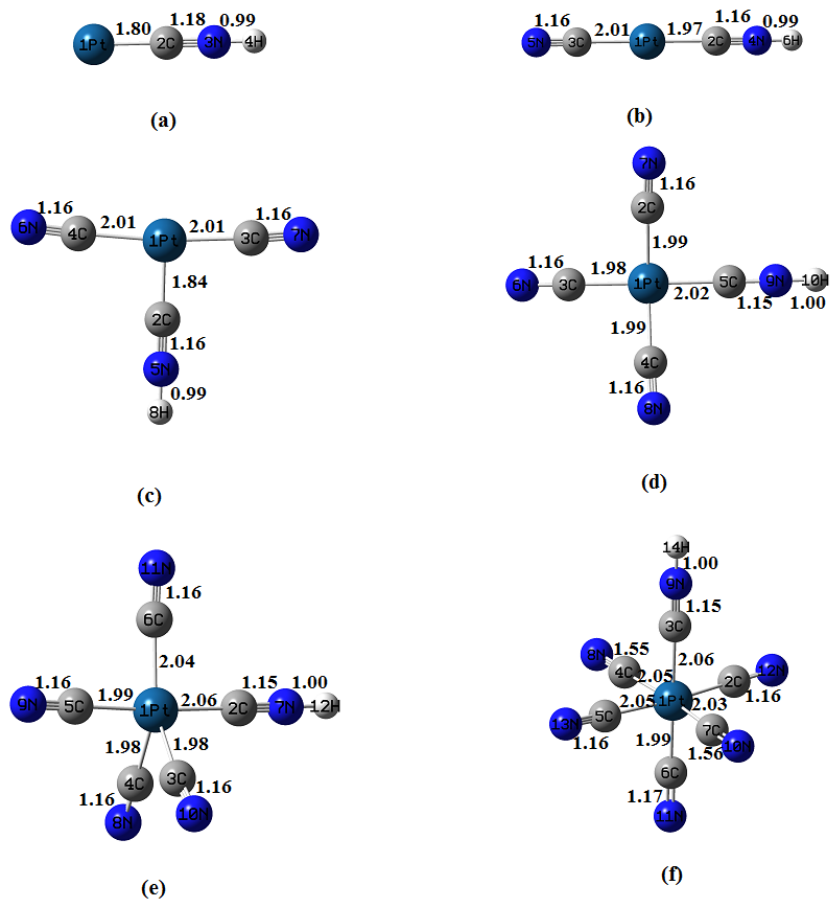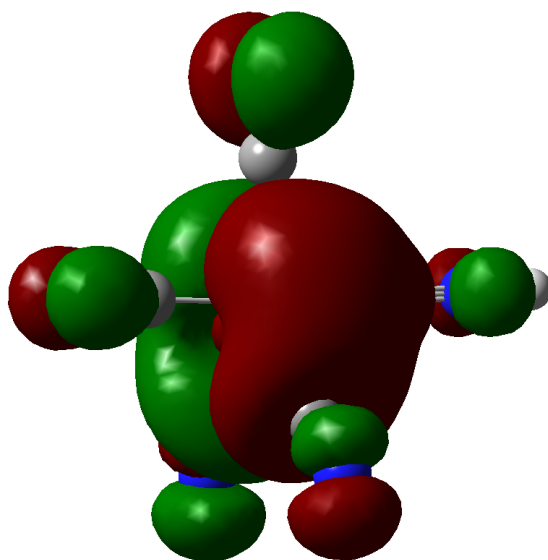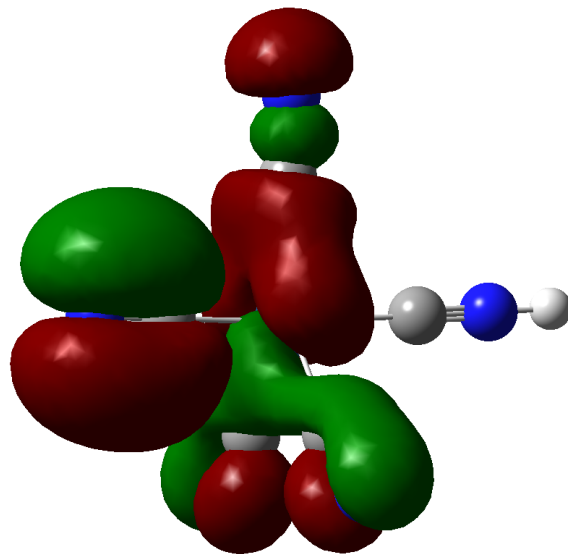
Figure 10. Equilibrium geometries of neutral H–Pt(CN)$_n$ ($n = 1$–6). Bond lengths (in Å) are also shown.

HOMO LUMO

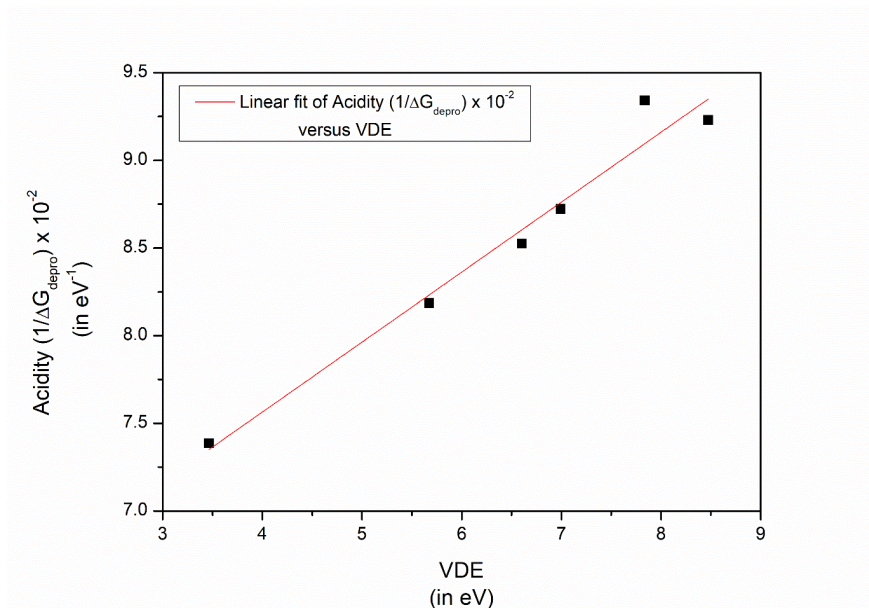Figure 11. HOMO–LUMO surfaces of H–Pt(CN)$_5$ superacid calculated using DFT (B3LYP) method.

Figure 12. Linear fitting plot of GPA $(1/[?]\text{G}_{\text{depro}}) \times 10^{-2}$ (in eV^{-1}) of H–Pt(CN)$_n$ species and VDE (in eV) of corresponding Pt(CN)$_n{}^-$ anions with correlation coefficient of $r = 0.9834$.